

# Self-assembled aggregates of amphiphilic perylene diimide-based semiconductor molecules: Effect of morphology on conductivity

Yanli Chen<sup>a,\*</sup>, Yajuan Feng<sup>a</sup>, Jian Gao<sup>a</sup>, Marcel Bouvet<sup>b</sup>

<sup>a</sup>Shandong Provincial Key Laboratory of Fluorine Chemistry and Chemical Materials, School of Chemistry and Chemical Engineering, University of Jinan, Jinan 250022, China

<sup>b</sup>Institut de Chimie Moléculaire de l'Université de Bourgogne, CNRS UMR 5260, Université de Bourgogne, 21078 Dijon, France

## ARTICLE INFO

### Article history:

Received 1 September 2011

Accepted 31 October 2011

Available online 10 November 2011

### Keywords:

Perylenetetracarboxy diimides

Self-assembly

Morphology

Molecular material

Conductivity

## ABSTRACT

Two amphiphilic perylenetetracarboxylic diimide derivatives modified with different side chains at imide nitrogen, *N*-*n*-hexyl-*N'*-(2-hydroxyethyl)-1,7-di(4'-*t*-butyl)phenoxy-peryene-3,4:9,10-tetracarboxylic diimide (**PDI 1**) and *N,N'*-di(2-hydroxyethyl)-1,7-di(4'-*t*-butyl)phenoxy-peryene-3,4:9,10-tetracarboxylic diimide (**PDI 2**), were fabricated into organic nanostructures via solution-phase self-assembly. Their self-assembling properties in methanol and *n*-hexane have been comparatively studied by electronic absorption, fluorescence, and Fourier transform infrared spectroscopy (FT-IR). The morphologies and structures of the self-assemblies were examined by scanning electronic microscopy (SEM), atomic force microscopy (AFM), as well as X-ray diffraction (XRD) techniques. The conducting properties were evaluated by current–voltage (*I*–*V*) measurements. Due to the presence of different number of hydroxyethyl groups in the molecule of **PDI 1** and **PDI 2**, the self-assembly of the two molecules in methanol and *n*-hexane results in nanostructures with distinctly different morphology as follows: nanobelts and nanoleaves for **PDI 1** and nanobelt dendrites and nanosheets for **PDI 2**, respectively. Analysis of the spectral change for the aggregates relative to that of monomeric **PDI** in solution revealed that in polar and apolar solvents, both nanobelts and nanoleaves precipitated from **PDI 1** adopt the *H* aggregation mode, whereas nanobelt dendrites and nanosheets from **PDI 2** adopt *H* and *J* aggregation mode, respectively, implying the effect of both side-chain substituent and solvent on tuning the intermolecular stacking. Furthermore, the conductivity of the aggregates of either **PDI 1** or **PDI 2** from methanol is more than ca. 1 order of magnitude higher than those from *n*-hexane. In particular, the well-defined, one-dimensional (1D) nanobelts of **PDI 1** show excellent semiconducting property with the electrical conductivity as high as  $3.3 \times 10^{-3} \text{ S cm}^{-1}$ , which might serve as promising candidates for applications in nano-electronics.

© 2011 Elsevier Inc. All rights reserved.

## 1. Introduction

Self-assembly of functional organic molecules with well-defined nanostructures based on various non-covalent interactions including  $\pi$ – $\pi$  interaction, van der Waals forces, hydrogen bonding, hydrophilic/hydrophobic interactions, electrostatic and metal–ligand coordination is important for the development of advanced functional molecular materials, nanoscale electronic and optoelectronic devices [1,2], such as OFETs [3], OLEDs [4], and sensors [5]. Intensive studies have led to the reports of various kinds of self-assembled organic nanostructures with different morphology such as nanowires [6–8], nanoribbons [9–11], nanorods [12], nanoparticles [13], and nanotubes [14,15]. However, the construction of organic nano-assembly into a prerequisite structure with controlled morphology depending on modifying the molecular structure and

programming the supramolecular interaction is still a challenge for chemists and material scientists.

As an important functional dye with outstanding photo and chemical stability as well as interesting photophysical and photochemical properties, perylenetetracarboxylic diimide derivatives (PDIs) have been intensively studied for several decades [4,16–19]. Because of their great potential application as organic semiconductors in different molecular electronic devices, the fabrication of ordered nanostructures with different morphology of this functional molecular material has become an attracting research area in the past decade [20–29]. Studies have revealed that the self-assembling process of PDI molecules is dominated by  $\pi$ – $\pi$  interaction between the conjugated perylene systems together with assistance of hydrogen bonding and side-chain hydrophobic interactions [30–33]. By introducing different side chains onto the imide positions of the PDI ring to tune the  $\pi$ – $\pi$  interaction between perylene systems, PDI nano-assemblies with different structure and morphology have been prepared by Zang and co-workers [34–37]. Würthner and co-workers have reported the

\* Corresponding author.

E-mail address: chm\_chenyl@ujn.edu.cn (Y. Chen).

self-assembling supramolecular structure of oligo(*p*-phenylene vinylene) (OPV)–PDI and OPV–PDI–OPV systems in methylcyclohexane driven by the hydrogen bonding and liquid crystal property and made corresponding characterization only on the basis of UV–vis method and molecular modeling [38,39]. Li and co-workers have observed the effect of dodecyloxy and/or thiododecyl groups at the bay positions on the structure and morphology of self-assembling PDI nanostructures [40]. Most of these PDI derivatives are symmetrically connected at the imide nitrogen atoms or the bay positions, and the nanostructural morphology was affected by the side chains. Very recently, aggregation behavior of a series of asymmetrical wedge-shaped PDIs has been reported by Li and co-workers [41]. However, to the best of our knowledge, a comparative investigation of the self-assembled nanostructures, morphology, and conductivity of resulting nanostructures between symmetrical and asymmetrical amphiphilic PDI derivatives is still rare. It is expected that when the two side chains have varied hydrophobicities/hydrophilicities, the morphology and microstructure may also be controlled not only by the molecular structure but also by the polarity of the solvents [42]. In this paper, two amphiphilic PDIs with different substituents linked at the imide positions of the perylene ring (Fig. 1), *N*-*n*-hexyl-*N'*-(2-hydroxyethyl)-1,7-di(4'-*t*-butyl)phenoxy-*perylene*-3,4:9,10-tetracarboxylic diimide (**PDI 1**) and *N,N'*-di(2-hydroxyethyl)-1,7-di(4'-*t*-butyl)phenoxy-*perylene*-3,4:9,10-tetracarboxylic diimide (**PDI 2**), were employed in our study, for the following reasons: (1) the conjugated frameworks can facilitate efficient  $\pi$ – $\pi$  electron delocalization and favor dense intermolecular  $\pi$ – $\pi$  stacking; (2) the introduction of functional groups having steric strain in the bay area of the perylene backbone (which can lead to a propeller-like twisting of the two naphthalene half units [43]) is expected to improve its solubility in conventional organic solvents, (3) the hydrophilic hydroxyethyl unit and/or hydrophobic linear alkyl chain linked at the imide nitrogen positions provide sufficient flexibility for the optimization of the non-covalent stacking of the PDI  $\pi$ -system by a balance between hydrogen bonding and hydrophobic interactions between the side chains of PDI molecules. A simple solution process allows us to prepare controllably large quantities of well-defined nanobelts and nanoleaves for **PDI 1** and nanobelt dendrites and nanosheets for **PDI 2**. In particular, one-dimensional (1D) nanobelts and nanobelt dendrites for **PDI 1** and **2** exhibited excellent conductivities. The investigation presented here demonstrates direct correlation between the maximized conductivity and the optimized molecular

stacking as well as the dimension of the self-assembly of PDI molecules.

## 2. Experimental section

### 2.1. Chemicals and measurements

All reagents and solvents were used as received. The asymmetric amphiphilic perylenetetracarboxylic diimide derivative, **PDI 1**, was used as synthesized previously [29]. The symmetric **PDI 2** was synthesized and purified according to published procedures [29,44,45]. The detailed synthetic procedures together with the structural characterization for **PDI 2** are described in [Supplementary material](#).

The nanostructures of the two compounds **PDI 1** and **2** were fabricated by the phase transfer method following the literature method [2,9,15,37]. A minimum volume (30–50  $\mu$ L) of concentrated chloroform solution of **PDI (1 and 2)** (1 mM) was injected rapidly into a large volume of methanol or *n*-hexane (1 mL) and subsequently mixed with a microinjector. After being kept at room temperature for 1–2 h, precipitates were separated from the solvents and transferred to the carbon-coated grid or SiO<sub>2</sub> surface for the SEM, AFM observations, and XRD measurement. Electronic absorption and fluorescence spectra were recorded on a Hitachi U-4100 spectrometer and a K2 system (ISS product), respectively. Fourier transform infrared (FT-IR) spectra were recorded as KBr pellets using a Bio-Rad FTS-165 spectrometer with 2 cm<sup>-1</sup> resolution. X-ray diffraction (XRD) experiment was carried out on a Rigaku D/max-B X-ray diffractometer. SEM images were obtained using a JEOL JSM-6700F field-emission scanning electron microscopy. For SEM imaging, Au (1–2 nm) was sputtered onto the grids to prevent charging effects and to improve the image clarity. Substrates used in the present study were successively cleaned with pure water, acetone, and ethanol.

### 2.2. Device fabrication

The interdigitated electrode (IDE) array is composed of 10 pairs of ITO electrode digits (fingers) deposited onto a glass substrate with the following dimensions: 125- $\mu$ m electrode width, 75- $\mu$ m spacing, 5850- $\mu$ m overlapping length, and 20-nm electrode thickness. The suspension of molecular aggregates was carefully dropped onto glass substrates with ITO IDEs. After complete evaporation of the solvents, the densely packed aggregates remained

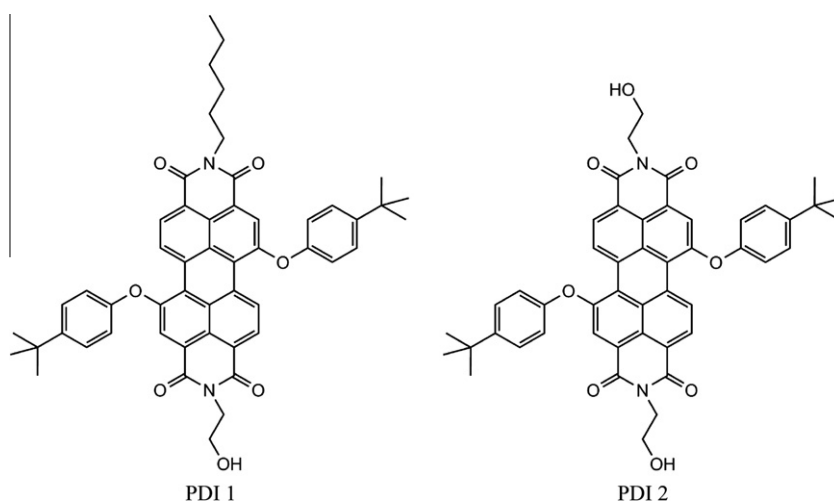


Fig. 1. The molecular structures of **PDI 1** and **PDI 2**.

and adhere to IDEs/glass substrate tightly (the process was repeated so that the channels of IDEs were completely covered by the aggregates), leading to the electron conductivity measurement in situ. The conductivity,  $\sigma$ , can be calculated according to the equation reported in the previous literatures [46,47]. The current–voltage characteristics were obtained using a Keithley 4200 semiconductor characterization system at room temperature in air.

### 3. Results and discussion

#### 3.1. Electronic absorption and fluorescence emission spectra

The electronic absorption and fluorescence emission spectra of the two PDI compounds in  $\text{CHCl}_3$  and their nano-aggregates fabricated in methanol and *n*-hexane are shown in Fig. 2, while the corresponding experimental data compiled in Table S1 (Supplementary material). As shown in Fig. 2A and B, both **PDI 1** and **PDI 2**, regardless of the different substituents on the imide N atoms of PDI cores, show just the same feature in their electronic absorption spectra, revealing the non-aggregated molecular spectroscopic nature of these two compounds in  $\text{CHCl}_3$ . In light of the previous observations as reported in the literature with regard to absorption characteristics of similar PDI derivatives [25,48,49], the absorptions at about 550 and 516 nm can be attributed to the 0–0 and 0–1 vibronic band of the  $S_0$ – $S_1$  transition, respectively, while the observed absorption band around 407 nm is attributed to the electronic  $S_0$ – $S_2$  transition. The fluorescence spectrum of either **PDI 1** or **PDI 2** in  $\text{CHCl}_3$  depicted the same peak structure and presented as a mirror image of the absorption, which gives no indication of aggregation, Fig. 2C and D. When dispersed in methanol or *n*-hexane, molecules of both **PDI 1**

and **2** undergo aggregation due to the limited solubility, which leads to distinctive change in their electronic absorption spectra (Fig. 2A and B). In comparison with those in  $\text{CHCl}_3$ , an enhanced 0–1 vibronic band along with a significant blueshift of the absorption maximum is observed in both methanol and *n*-hexane, Fig. 2A. Meantime, a new band emerges around 650 nm for the aggregates of **PDI 1**. Such a spectral change implies strong molecular stacking between the PDI skeletons and the formation of face-to-face  $\pi$  stacks (*H*-aggregate) [43]. The pronounced absorption band emerging at longer wavelength is typically a sign of the effective  $\pi$ – $\pi$  interaction in co-facial configuration of molecular stacking [36,37,43]. Consistent with the absorption measurement, the emission spectrum of the aggregates of **PDI 1** also shows a blueshift of the emission maxima by 3 and 18 nm in methanol and *n*-hexane as compared to that in solution, respectively, Fig. 2C. One new emission band at approximately 690 nm for the aggregates of **PDI 1** in both “poor” solvents should be attributed to emission from the excimer-like states of the molecular aggregates formed by the interaction between adjacent **PDI 1** molecules in the co-facial arrangement [25,42]. It is noteworthy that the blue-shifted extent of both emission and absorption peaks of the aggregates of **PDI 1** increases with the decrease in the solvent polarity, which is in good agreement with a study on the self-assembled behavior of an asymmetrical amphiphilic PDI derivative reported by Ji and co-workers [42]. The UV–vis absorption spectra and fluorescence emission spectra for a diluted suspension of molecular aggregate of **PDI 2** in methanol and *n*-hexane are also shown in Fig. 2B and D, respectively, which are different from that of **PDI 2** in  $\text{CHCl}_3$  solution due to the significant intermolecular interaction in the self-assembled nanostructures. In comparison with the spectrum of **2** in chloroform, self-assembled **PDI 2** shows a blueshift on the maximum absorp-

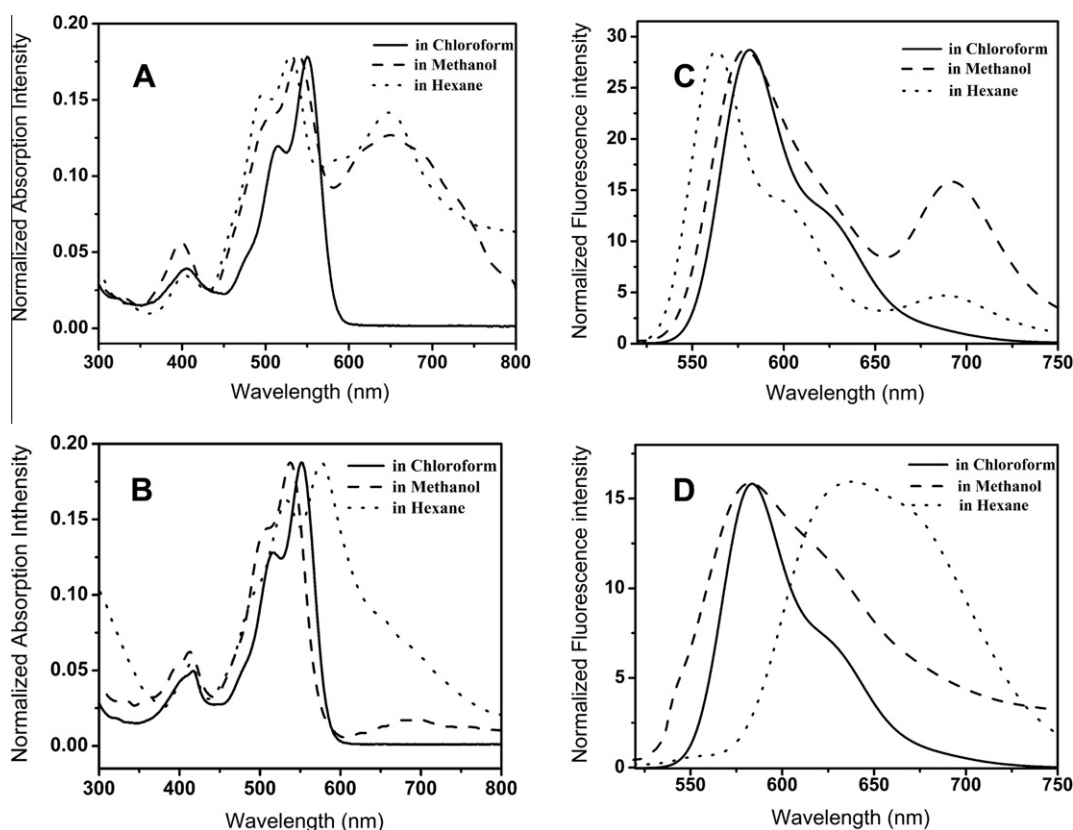


**Fig. 2.** Normalized electronic absorption (left) and fluorescence emission (right) spectra of **PDI 1** (A and C) and **PDI 2** (B and D) in chloroform (solid line) and their nanostructures dispersed in methanol (dashed line) and *n*-hexane (dotted line). The excited wavelength was 510 nm.

tion band in methanol and a redshift in *n*-hexane, corresponding to the *H*- and *J*-type aggregates, respectively, which imply directly the effect of the solvent on the molecular packing mode [42]. The different self-assembly behavior for the asymmetric **PDI 1** and symmetric **PDI 2** in polar and apolar solvents also indicates the different effects of the solvent–PDI molecules interaction during the self-assembly process, which counterbalances the PDI intermolecular interaction, in particular the hydrogen bonding between the hydroxyethyl groups and hydrophobic interaction between alkyl chains, on the molecular packing mode. Further evidence for this point comes from FT-IR and XRD experimental result as detailed below.

### 3.2. FT-IR spectra

The FT-IR spectra of the self-assembled nanostructures of **PDI 1** and **2** obtained from methanol and *n*-hexane are shown in Figs. S1 and S2, respectively (Supplementary material). The positions of the peak frequencies for the CH<sub>2</sub> symmetrical ( $\nu_s(\text{CH}_2)$ ) and anti-symmetrical ( $\nu_a(\text{CH}_2)$ ) stretching vibrations provide insight into the intermolecular environment of the alkyl chains in these assemblies. Previous IR studies have shown that the location of these peaks can be a sensitive indicator for the extent of the lateral interactions between long *n*-alkyl and polymethylene chains [50,51]. For example, the **PDI 1** self-assembled nano-aggregates from both methanol and *n*-hexane showed the  $\nu_s(\text{CH}_2)$  and  $\nu_a(\text{CH}_2)$  at ca. 2854 and 2922 cm<sup>-1</sup>, respectively (Fig. S1), which are almost the same positions as those reported in the literature [46], indicating that the long alkyl chains are stretched to form a multilayer tape via interdigitation [46,50,51]. For the aggregates of **PDI 2**, the vibration bands at ca. 2850 and 2917 cm<sup>-1</sup> are assigned to the  $\nu_s(\text{CH}_2)$  and  $\nu_a(\text{CH}_2)$  modes, respectively (Fig. S2). Obviously, the peak frequencies for both  $\nu_s(\text{CH}_2)$  and  $\nu_a(\text{CH}_2)$  modes of **PDI 2** aggregates are lower than those of **PDI 1** aggregates by 4–5 cm<sup>-1</sup>, respectively. Therefore, the side chains in **PDI 2** aggregates are more ordered than those of **PDI 1** [52,53]. In addition, the presence of a relatively broad and strong band appearing in the range of 3437–3463 cm<sup>-1</sup> as shown in Figs. S1 and S2, respectively, is assigned to the stretching vibration of hydrogen bonds between the hydroxyethyl groups attached to imide nitrogen position(s) of neighboring PDI molecules [2,54,55]. This is in line with the X-ray diffraction (XRD) result as detailed below.

### 3.3. X-ray diffraction patterns of the aggregates

The internal structure of self-assembled nanostructures of these compounds was investigated by XRD analysis. As shown in Fig. 3A, in the low angle range, the XRD diagram of the nanostructures of **PDI 1** formed from methanol shows two clear diffraction peaks at  $2\theta = 4.18^\circ$  (2.11 nm) and  $4.80^\circ$  (1.84 nm), which are ascribed to the diffractions from the (100) and (010) planes, respectively [56]. As can be seen from Fig. 3C, the dimensional size of a **PDI 1** molecule is ca. 2.24 nm (length)  $\times$  1.50 nm (width)  $\times$  0.78 nm (thickness) obtained from the energy-optimized structure of the molecule by using Gaussian 98 program at B3LYP/6-31G(d) level. According to the XRD result and the simulated **PDI 1** molecular structure, the unit cell consists of six **PDI 1** molecules, Fig. 3D. The d-spacing of 2.11 and 1.84 nm could be attributed to the average length along the long axis of **PDI 1** and the thickness along the perpendicular direction to the perylene rings, respectively. In addition, two higher-order diffractions are found at 1.05 and 0.94 nm, corresponding to (200) and (020) plane, respectively, which means that there exists very regular repetition of the nanostructure along the long axis of the PDI as well as the direction perpendicular to the perylene rings, despite the fact that this is solely based on the non-covalent interactions. It is worth noting that, in the wide angle region, the XRD pattern of **PDI 1** nanostructures formed from methanol presents additional diffraction at 0.33 and 0.26 nm, which can be attributed to the  $\pi$ - $\pi$  stacking distance of PDI rings between the adjacent molecules [26,27] and the distance between hydrogen-bonding hydroxyl oxygens [2]. Almost the same diffraction peaks (at 0.32 and 0.27 nm) are also obtained for **PDI 1** aggregates formed from *n*-hexane, which is in good accordance with the results of electronic absorption and IR spectroscopy. However, in the low angle region, the XRD pattern of **PDI 1** aggregates formed from *n*-hexane presents only a comparatively strong and sharp diffraction peak at 1.85 nm (Fig. 3B), which is ascribed to the diffractions from the (010) plane, implying a favorable molecular packing from co-facial conformation depending mainly on the  $\pi$ - $\pi$  interaction between perylene rings. For the **PDI 1** aggregates from *n*-hexane, the (100) diffraction observed at 2.11 nm for the **PDI 1** nanostructures from methanol was absent, suggesting the lack of long-range periodicity along this direction in the self-assembled nanostructures of this PDI compound. Obviously, such a difference in XRD pattern should attributed to the different polarity of *n*-hexane and methanol. Although both

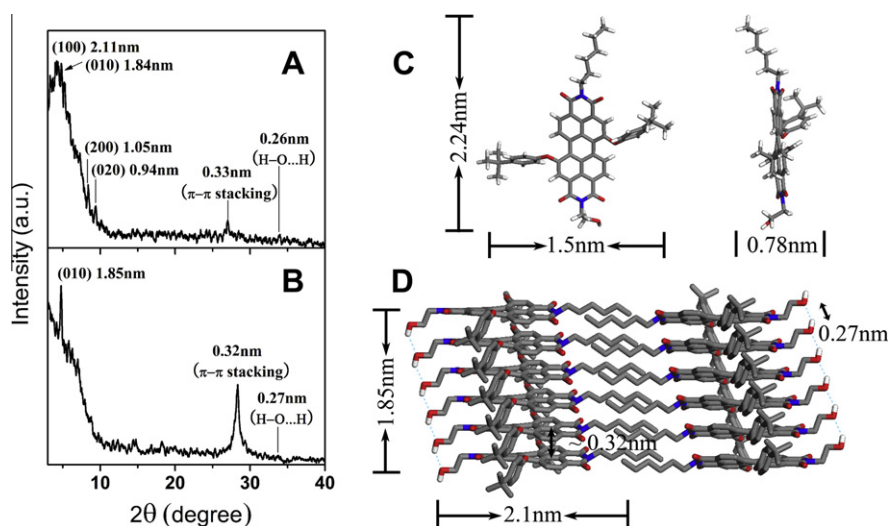


**Fig. 3.** X-ray diffraction patterns of the nanostructures of **PDI 1** from methanol (A); *n*-hexane (B); molecular size of **PDI 1** obtained from DFT calculation at the B3LYP/6-31G(d) level (C); and schematic representation of the unit cell in the nanostructure of **PDI 1** (D).

solvents provide limited solubility for **PDI 1** and thus facilitate the molecular aggregation, the stronger solvent–molecule interaction between *n*-hexane and the hexyl group may reduce the interdigitation between the side chains of **PDI 1**. As a consequence, growth in this direction during the self-assembly process is limited. The different favorable growing orientations of aggregates of **PDI 1** from methanol and *n*-hexane in turn result in the different morphology as detailed below.

The XRD patterns of self-assembled nanostructures of **PDI 2** formed from methanol show one comparatively strong and sharp diffraction peak at 1.63 nm along with another weaker diffraction at 1.43 nm in the low angle range, originating from the (010) and (001) planes, respectively, Fig. 4A. These two diffraction peaks should be assigned to the dimensional size for a unit cell, 1.63 nm (thickness)  $\times$  1.43 nm (width), formed from co-facial stacking of six **PDI 2** molecules depending on the  $\pi$ - $\pi$  stacking and the intermolecular hydrogen bonds of neighboring PDI molecules, on the basis of the energy-optimized structure of the molecule, Fig. 4C. Very interesting, the (010) and (001) diffraction peaks for aggregates of **PDI 2** from *n*-hexane were at the almost same position as those of **PDI 2** from methanol except a reversed relative intensity (Fig. 4A and B), implying the different favorable growing orientations of nanostructures of **PDI 2** in polar and apolar solvent. As a result, molecules assembled along the perpendicular and transverse direction of perylene rings [43], respectively (Fig. 4D and E), according to the energy-optimized, three-dimensional size of a **PDI 2** molecule. This is well reflected by the difference in the *H* versus *J* aggregation mode observed by UV–vis absorption spectra as detailed above. In the wide angle region, the peaks at 0.31 and 0.26 nm are also observed, which are assigned just in the same way as done for the aggregates of **PDI 1**.

#### 3.4. Morphology of the aggregates

The morphology of the aggregates formed was examined by scanning electron microscopy (SEM) and atomic force microscopy (AFM). Fig. 5 displays typical scanning electronic microscopy (SEM) images of **PDI 1** formed from methanol and *n*-hexane. In methanol, **PDI 1** assembled into nanostructures with belt-like morphology with uniform size and orientation, Fig. 5A and B. The nanobelts were ordered over 50  $\mu\text{m}$  in length with average width of ca. 2  $\mu\text{m}$ . The belt morphology was also revealed by the AFM

measurement, as shown in Fig. S3A. The line-scan profile over a single belt demonstrates a flat topography typical of a nanobelt with a thickness of around 330 nm, Fig. S3B, and an aspect ratio (length over thickness) larger than 150. This is favorable for the device application in photovoltaics and field effect transistors [57]. Unlike the aggregates in methanol, the aggregates of **PDI 1** in *n*-hexane present a leaf-like morphology of ca. 2  $\mu\text{m}$  in length around 500 nm in width (Fig. 5C and D) and 70 nm in thickness (Fig. S3C and D), leading to an aspect ratio (length over thickness) of 29. The similar solvent effect was also observed in the self-assembly of **PDI 2**. In methanol, **PDI 2** molecules self-assemble into nanobelts (Fig. 5E and F). The belts are usually about 0.2–1  $\mu\text{m}$  in width and 20–25  $\mu\text{m}$  in length (and 40 nm in thickness, Fig. S4A and B). Two nanobelts are often linked together to form Y-junctions (Fig. 5F) [14,58], which in turn construct more complicated junctions, for instance, the dendrite composed of nanobelt branches, in which each nanobelt spreads out from its root and acts as a branch. However, in *n*-hexane, self-assembly of **PDI 2** results in nanostructures with a quadrate sheet-like morphology with about 0.5–1.6  $\mu\text{m}$  in width, 3–5  $\mu\text{m}$  in length, and 210 nm in thickness, Figs. 5G and H and S4C and D. Obviously, nanostructures of both **PDI 1** and **PDI 2** from methanol show higher aspect ratio than those from *n*-hexane. Self-assembly morphology of the PDI amphiphiles is determined not only by the molecular structure but also by the intermolecular interactions between the amphiphiles as well as the interactions between the amphiphiles and solvent. It is worth noting that the size- and morphology-adjustable nanostructures are highly desired for fabricating nanoscale molecular (opto)-electronic devices that often require a wide variety of channel lengths to achieve the optimum gate or optical modulation.

#### 3.5. *I*-*V* properties

The uniform aggregates of **PDI 1** and **2** with well-defined nanostructures would be promising candidates for applications in electronic devices. To demonstrate the potentials of these nanostructures, the diluted suspension of molecular aggregates of **PDI 1** and **2** formed in methanol and *n*-hexane was carefully dropped onto glass substrates with ITO IDEs, respectively. After complete evaporation of the solvents, the densely packed nanostructural films remained and adhere to ITO IDEs/glass substrate tightly, leading to the electron conductivity measurement in situ. Fig. 6 shows

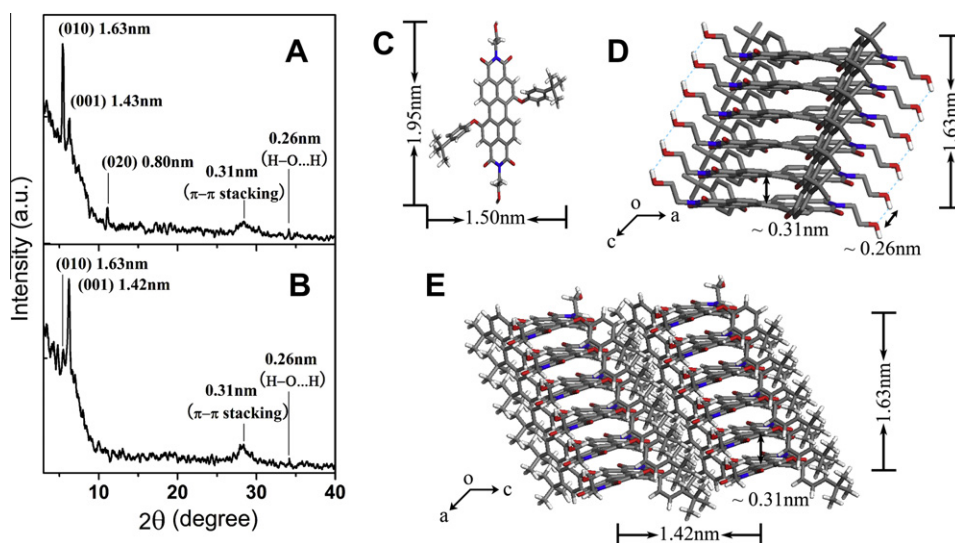


**Fig. 4.** X-ray diffraction patterns of the nanostructures of **PDI 2** from methanol (A); from *n*-hexane (B); molecular size of **PDI 2** obtained from DFT calculation at the B3LYP/6-31G(d) level (C); and schematic representation of the unit cell in the nanostructure of **PDI 2** (D and E).

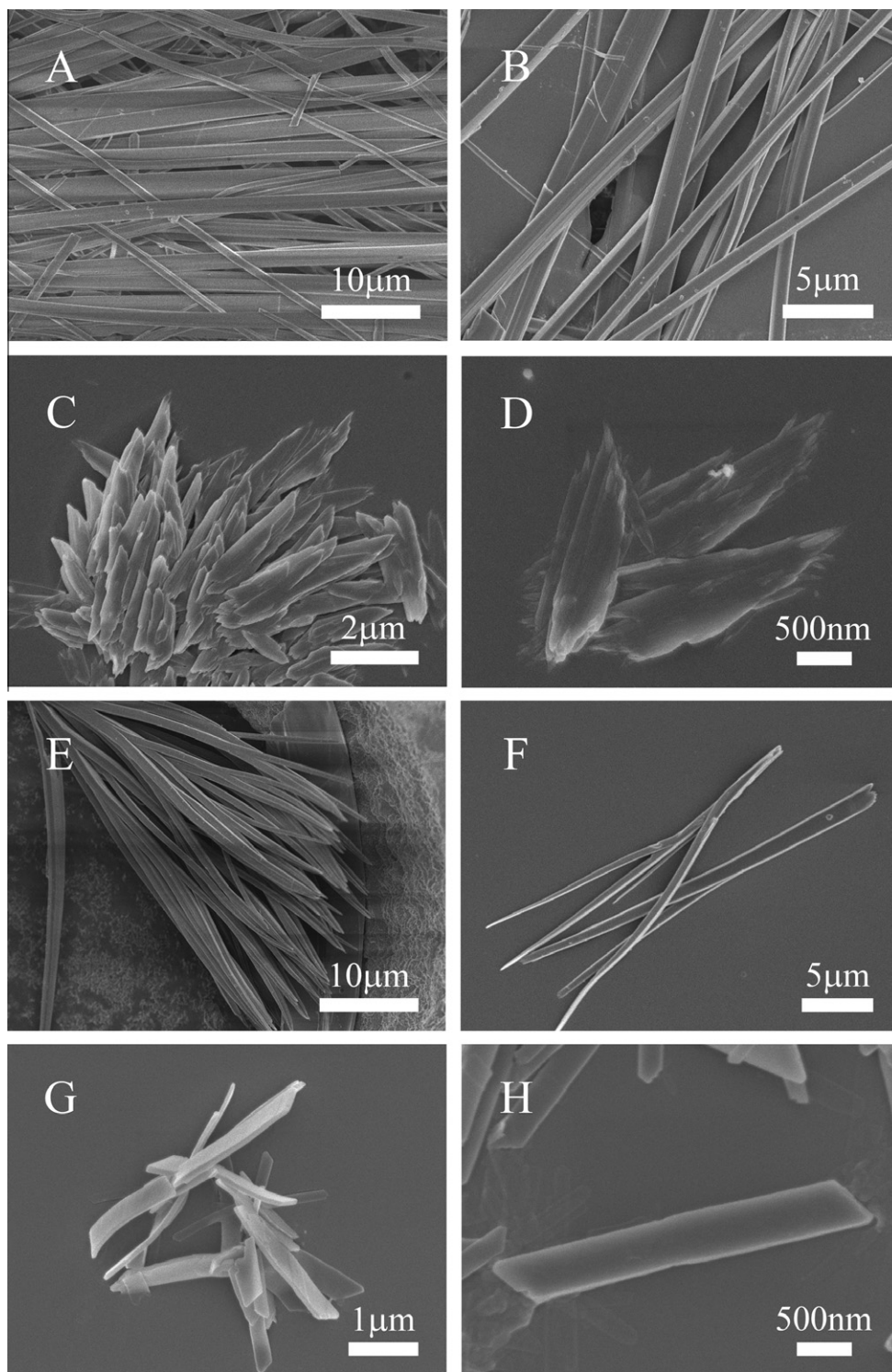


**Fig. 5.** SEM images of the nanobelts from methanol (A and B) and nanoleaves from *n*-hexane (C and D) for **PDI 1**; nanobelt dendrites from methanol (E and F) and nanosheets from *n*-hexane (G and H) for **PDI 2**, respectively.

the current–voltage (*I*–*V*) characteristics of nanobelts and nanoleaves of **PDI 1** and nanobelt dendrites and nanosheets of **PDI 2**. The devices made from different nanostructural films of both **PDI 1** and **2** exhibited similar conductive behavior: conductivity increased in the order of aggregates from *n*-hexane < aggregates from methanol. The higher the one-dimensional order, the higher the mobility of charge carriers and conductivity. This trend in conducting performance has previously been observed for porphyrins,

phthalocyanines, and amphiphilic hexa-peri-hexabenzocoronene materials [14,46,51]. According to the equation reported in the literatures [46,47], the electronic conductivity is calculated to be around  $3.3 \times 10^{-3}$  and  $1.2 \times 10^{-4} \text{ S cm}^{-1}$  for the nanobelts and nanoleaves of **PDI 1**, and  $2.8 \times 10^{-4}$  and  $3.0 \times 10^{-5} \text{ S cm}^{-1}$  for nanobelt dendrites and nanosheets of **PDI 2**, respectively (the experiments were repeated for more than three times on different pieces of films). Comparing with nanosheets for **PDI 2**, the

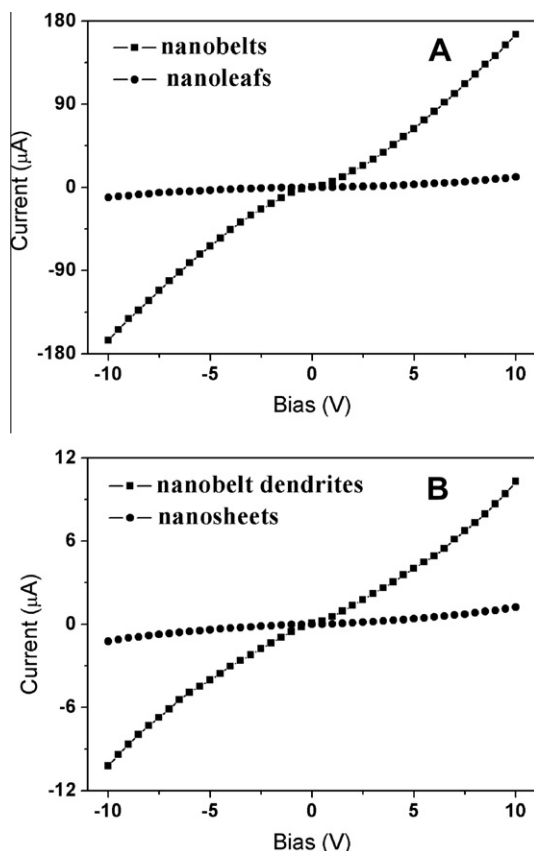


**Fig. 6.** *I*–*V* curves measured on nanobelts (solid squares) and nanoleaves (solid circles) from **PDI 1** (A), nanobelt dendrites (solid squares) and nanosheets (solid circles) from **PDI 2** (B).

dramatically improved conductivity of nanobelt dendrites for **PDI 2** might be due to the long-range 1D  $\pi$ – $\pi$  stacking structure that favors the conductivity through face-to-face intermolecular  $\pi$ -delocalization (Fig. 6B). The extra high conductivity (ca.  $3.3 \times 10^{-3} \text{ S cm}^{-1}$ ) was measured for the **PDI 1** nanobelts, which is about 3 order of magnitude higher than that measured from polymer nanowires (e.g. polythiophene) [59]. This unexpected good conductivity of the nanobelts of **PDI 1** might be attributed to both readily  $\pi$ -stacks with adjacent planar molecules and higher-ordered crystalline molecular arrangement. When the perylene cores are organized in one-dimensional stacks in nanobelts, they may show favorable charge transport [60]. The absence of traps and/or defects in these one-dimensional aggregates with more efficient  $\pi$ -stacks and side-chain interactions should favor charge transport. This solid-state packing effect has been previously suggested in explaining the OFET behavior for highly crystalline *n*-channel organic TCTDT [6] and TFTs [61]. It is worth noting that the conductivity of the aggregates of either **PDI 1** or **PDI 2** from methanol is more than ca. 1 order of magnitude higher than those from *n*-hexane, implying the significant effect of the intermolecular interaction and the molecular packing mode in aggregates associated with the solvent–PDI molecular interaction on the conductivity. These aggregates with such high current modulation could be useful for a wide range of electronic and sensor devices. The efforts to explore such opportunities are underway.

#### 4. Summary

Aggregates with distinct morphologies and structures for **PDI 1** and **PDI 2** were controllably prepared in polar and apolar solvent,

respectively. The *I*–*V* experimental results revealed that the present PDI molecules might serve as the useful functional materials for nano-electronics. The present study represents our new effort toward preparing self-assembled microstructures with controlled morphology and properties through both molecular modification and the solvent effect. It will be valuable for the design and preparation of PDI-based nano-electronic and nano-optoelectronic devices with good performance due to the close relationship between the molecular ordering and dimensions of nanostructures and the performance of nanodevices.

#### Acknowledgments

Financial support from the Natural Science Foundation of China (20871055), Natural Science Foundation of Shandong Province (ZR2011BZ005), and University of Jinan in China is gratefully acknowledged.

#### Appendix A. Supplementary material

Supplementary data associated with this article can be found, in the online version, at doi:10.1016/j.jcis.2011.10.076.

#### References

- [1] J.A.A.W. Elemans, R. van Hameren, R.J.M. Nolte, A.E. Rowan, *Adv. Mater.* 18 (2006) 1251.
- [2] G. Lu, Y. Chen, Y. Zhang, M. Bao, Y. Bian, X. Li, J. Jiang, *J. Am. Chem. Soc.* 130 (2008) 11623.
- [3] G. Horowitz, F. Kouki, P. Spearman, D. Fichou, C. Nogue, X. Pan, F. Garnier, *Adv. Mater.* 8 (1996) 242.
- [4] B.A. Jones, M.J. Ahrens, M.-H. Yoon, A. Facchetti, T.J. Marks, M.R. Wasielewski, *Angew. Chem. Int. Ed.* 43 (2004) 6363.
- [5] M. Bouvet, H. Xiong, V. Parra, *Sens. Actuators, B: Chem.* 145 (2010) 501.
- [6] X. Mu, W. Song, Y. Zhang, K. Ye, H. Zhang, Y. Wang, *Adv. Mater.* 22 (2010) 4905.
- [7] H. Gan, H. Liu, Y. Li, Q. Zhao, Y. Li, S. Wang, T. Jiu, N. Wang, X. He, D. Yu, D. Zhu, *J. Am. Chem. Soc.* 127 (2005) 12452.
- [8] G. Lu, X. Zhang, X. Cai, J. Jiang, *J. Mater. Chem.* 19 (2009) 2417.
- [9] Y. Gao, Y. Chen, R. Li, Y. Bian, X. Li, J. Jiang, *Chem. Eur. J.* 15 (2009) 13241.
- [10] Y. Gao, X. Zhang, C. Ma, X. Li, J. Jiang, *J. Am. Chem. Soc.* 130 (2008) 17044.
- [11] W. Lv, X. Wu, Y. Bian, J. Jiang, X. Zhang, *ChemPhysChem* 10 (2009) 2725.
- [12] A.D. Schwab, D.E. Smith, B. Bond-Watts, D.E. Johnston, J. Hone, A.T. Johnson, J.C. de Paula, W.F. Smith, *Nano Lett.* 4 (2004) 1261.
- [13] X. Gong, T. Milic, C. Xu, J.D. Batteas, C.M. Drain, *J. Am. Chem. Soc.* 124 (2002) 14290.
- [14] Z. Wang, C.J. Medforth, C.J. Shelnut, *J. Am. Chem. Soc.* 126 (2004) 15954.
- [15] P. Ma, Y. Chen, Y. Bian, J. Jiang, *Langmuir* 26 (2010) 3678.
- [16] B.A. Gregg, R.A. Cormier, *J. Am. Chem. Soc.* 123 (2001) 7959.
- [17] C.W. Struijk, A.B. Sieval, E.J.J. Dakhorst, M. van Dijk, P. Kimkes, R.B.M. Koehorst, H. Donker, T.J. Schaafsma, S.J. Picken, A.M. van de Craats, J.M. Warman, H.E. Zuihof, J.R. Sudholter, *J. Am. Chem. Soc.* 122 (2000) 11057.
- [18] P. Ranke, I. Bleyl, J. Simmerer, D. Haarer, A. Bacher, H.W. Schmidt, *Appl. Phys. Lett.* 71 (1997) 1332.
- [19] X. Li, L.E. Sinks, B. Rybtchinski, M.R. Wasielewski, *J. Am. Chem. Soc.* 126 (2004) 10810.
- [20] T. van der Boom, R.T. Hayes, Y. Zhao, P.J. Bushard, E.A. Weiss, M.R. Wasielewski, *J. Am. Chem. Soc.* 124 (2002) 9582.
- [21] M.J. Fuller, L.E. Sinks, B. Rybtchinski, J.M. Giaimo, X. Li, M.R. Wasielewski, *J. Phys. Chem. A* 109 (2005) 970.
- [22] B. Rybtchinski, L.E. Sinks, M.R. Wasielewski, *J. Am. Chem. Soc.* 126 (2004) 12268.
- [23] F. Würthner, Z. Chen, V. Dehm, V. Stepanenko, *Chem. Commun.* (2006) 1188.
- [24] F. Würthner, *Pure Appl. Chem.* 78 (2006) 2341.
- [25] F. Würthner, C. Thalacker, S. Diele, C. Tschierske, *Chem. Eur. J.* 7 (2001) 2245.
- [26] Z. Chen, U. Baumeister, C. Tschierske, F. Würthner, *Chem. Eur. J.* 13 (2007) 450.
- [27] Z. Chen, V. Stepanenko, V. Dehm, P. Prins, L.D.A. Siebbeles, J. Seibt, P. Marquetand, V. Engel, F. Würthner, *Chem. Eur. J.* 13 (2007) 436.
- [28] Y. Chen, Y. Kong, Y. Wang, P. Ma, M. Bao, X. Li, *J. Colloid Interface Sci.* 330 (2009) 421.
- [29] Y. Chen, L. Chen, G. Qi, H. Wu, Y. Zhang, L. Xue, P. Zhu, P. Ma, X. Li, *Langmuir* 26 (2010) 12473.
- [30] C. Thalacker, F. Würthner, *Adv. Funct. Mater.* 12 (2002) 209.
- [31] L.E. Sinks, B. Rybtchinski, M. Iimura, B.A. Jones, A.J. Goshe, X. Zuo, D.M. Tiede, X. Li, M.R. Wasielewski, *Chem. Mater.* 17 (2005) 6295.
- [32] A. Sautter, C. Thalacker, F. Würthner, *Angew. Chem. Int. Ed.* 40 (2001) 4425.
- [33] S. Ghosh, X.-Q. Li, V. Stepanenko, F. Würthner, *Chem. Eur. J.* 14 (2008) 11343.
- [34] Y. Che, X. Yang, S. Loser, L. Zang, *Nano Lett.* 8 (2008) 2219.
- [35] L. Zang, Y. Che, J.S. Moore, *Acc. Chem. Res.* 41 (2008) 1596.

- [36] K. Balakrishnan, A. Datar, R. Oitker, H. Chen, J. Zuo, L. Zang, *J. Am. Chem. Soc.* 127 (2005) 10496.
- [37] K. Balakrishnan, A. Datar, T. Naddo, J. Huang, R. Oitker, M. Yen, J. Zhao, L. Zang, *J. Am. Chem. Soc.* 128 (2006) 7390.
- [38] E.H.A. Beckers, S.C.J. Meskers, A.P.H.J. Schenning, Z. Chen, F. Würthner, P. Marsal, D. Beljonne, J. Cornil, R.A.J. Janssen, *J. Am. Chem. Soc.* 128 (2005) 649.
- [39] E.H.A. Beckers, Z. Chen, S.C.J. Meskers, P. Jonkheijm, A.P.H.J. Schenning, X. Li, P. Osswald, F. Würthner, R.A.J. Janssen, *J. Phys. Chem. B* 110 (2006) 16967.
- [40] W. Su, Y. Zhang, C. Zhao, X. Li, J. Jiang, *ChemPhysChem* 8 (2007) 1857.
- [41] L. Xue, Y. Wang, Y. Chen, X. Li, *J. Colloid Interface Sci.* 350 (2010) 523.
- [42] X. Yang, X. Xu, H.-F. Ji, *J. Phys. Chem. B* 112 (2008) 7196.
- [43] S. Vajiravelu, L. Ramunas, G.J. Vidas, G. Valentas, J. Vygintas, S. Valiyaveetil, *J. Mater. Chem.* 19 (2009) 4268.
- [44] C. Zhao, Y. Zhang, R. Li, X. Li, J. Jiang, *J. Org. Chem.* 72 (2007) 2402.
- [45] Y. Wang, Y. Chen, R. Li, S. Wang, W. Su, P. Ma, M.R. Wasielewski, X. Li, *J. Langmuir* 23 (2007) 5836.
- [46] Y. Chen, M. Bouvet, T. Sizun, Y. Gao, C. Plassard, E. Lesniewska, J. Jiang, *Phys. Chem. Chem. Phys.* 12 (2010) 12851.
- [47] H. Ahn, A. Chandekar, B. Kang, C. Sung, J.E. Whitten, *Chem. Mater.* 16 (2004) 3274.
- [48] M.R. Wasielewski, *Acc. Chem. Res.* 42 (2009) 1910.
- [49] F. Würthner, *Chem. Commun.* (2004) 1564.
- [50] J.P. Hill, W. Jin, A. Kosaka, T. Fukushima, H. Ichihara, T. Shimomura, K. Ito, T. Hashizume, N. Ishii, T. Aida, *Science* 304 (2004) 1481.
- [51] Y. Yamamoto, T. Fukushima, Y. Sun, N. Ishii, A. Saeki, S. Seki, S. Tagawa, M. Taniguchi, T. Kawai, T. Aida, *Science* 314 (2006) (1761).
- [52] T. Nakanishi, B. Ohtani, K. Uosaki, *J. Phys. Chem. B* 102 (1998) 1571.
- [53] C. Zhan, P. Gao, M. Liu, *Chem. Commun.* (2005) 462.
- [54] M. Kimura, T. Muto, H. Takimoto, K. Wada, K. Ohta, K. Hanabusa, H. Shirai, N. Kobayashi, *Langmuir* 16 (2000) 2078.
- [55] M. Kimura, T. Kuroda, K. Ohta, K. Hanabusa, H. Shirai, N. Kobayashi, *Langmuir* 19 (2003) 4825.
- [56] D. Schlettwein, H. Graaf, J.-P. Meyer, T. Oekermann, N.I. Jaeger, *J. Phys. Chem. B* 103 (1999) 3078.
- [57] A. Babel, S.A. Jenekhe, *J. Am. Chem. Soc.* 125 (2005) 13656.
- [58] S. Guo, E. Wang, *Langmuir* 24 (2008) 2128.
- [59] G.A. O'Brien, A.J. Quinn, D.A. Tanner, G. Redmond, *Adv. Mater.* 18 (2006) 2379.
- [60] R. Kella, A. Serra, P. Siciliano, A. Tepore, L. Valli, A. Zocco, *Langmuir* 13 (1997) 6562.
- [61] A.L. Briseno, S.C.B. Mannsfeld, C. Reese, J.M. Hancock, Y. Xiong, S.A. Jenekhe, Z. Bao, Y. Xia, *Nano Lett.* 7 (2007) 2847.